LA-UR-16-22984 (Accepted Manuscript)

Spall fracture in additive manufactured Ti-6Al-4V

Jones, David Robert
Fensin, Saryu Jindal
Dippo, Olivia
Beal, Roberta Ann
Livescu, Veronica
Martinez, Daniel Tito
Trujillo, Carl Patrick
Gray, George Thompson III

To be published in: Journal of Applied Physics

DOI to publisher's version: 10.1063/1.4963279

Permalink to record: http://permalink.lanl.gov/object/view?what=info:lanl-repo/lareport/LA-UR-16-22984

Spall Fracture in Additive Manufactured Ti-6Al-4V

D R Jones,[1, a)] S J Fensin,[1] O Dippo,[1] R A Beal,[1] V Livescu,[1] D T Martinez,[1] C P Trujillo,[1] J N Florando,[2] M Kumar,[2] and G T Gray III[1]

[1)] *MST-8, Los Alamos National Laboratory, Los Alamos, NM 87545, USA*

[2)] *Lawrence Livermore National Laboratory, Livermore, CA 94550, USA*

(Dated: 13 October 2016)

We present a study on the spall strength of additive manufactured (AM) Ti-6Al-4V. Samples were obtained from two pieces of selective laser melted (SLM, a powder bed fusion technique) Ti-6Al-4V such that the response to dynamic tensile loading could be investigated as a function of the orientation between the build layers and the loading direction. A sample of wrought bar-stock Ti-6Al-4V was also tested to act as a baseline representing the traditionally manufactured material response. A single-stage light gas-gun was used to launch a thin flyer plate into the samples, generating a region of intense tensile stress on a plane normal to the impact direction. The rear free surface velocity time history of each sample was recorded with laser-based velocimetry to allow the spall strength to be calculated. The samples were also soft recovered to enable post-mortem characterization of the spall damage evolution. Results showed that when the tensile load was applied normal to the interfaces between the build layers caused by the SLM fabrication process the spall strength was drastically reduced, dropping to 60 percent of that of the wrought material. However, when loaded parallel to the AM build layer interfaces the spall strength was found to remain at 95 percent of the wrought control, suggesting that when loading normal to the AM layer interfaces, void nucleation is facilitated more readily due to weaknesses along these boundaries. Quasi-static testing of the same sample orientations revealed a much lower degree of anisotropy, demonstrating the importance of rate-dependent studies for damage evolution in AM materials.

Keywords: Additive manufacturing, powder bed fusion, selective laser melting, Ti-6Al-4V, plate impact, spall fracture

I. INTRODUCTION

Additive manufacturing (AM) allows components with complex geometries to be produced that would be otherwise impossible with conventional production methods such as machining or casting.[1] One AM technique that is becoming widely used with engineering materials such as steel and titanium alloys is powder bed fusion, one method of which is selective laser melting (SLM). This involves a laser scanning across a bed of powder, illuminating certain areas where the powder melts and subsequently fuses together to create a slice of the desired final part. A new layer of powder is then spread over this fused layer and the process repeats, building the part in layers that are typically on the order of 10 µm to 100 µm in thickness.[2] The rapid heating by the laser and the quenching by the surrounding powder can introduce large thermal stresses and microstructures not usually produced in wrought conventionally machined parts.[3] While there is a growing body of research into the behavior of SLM materials subjected to quasi-static loading[4–9], there is a very limited amount of data on their behavior at higher strain rates,[10] especially under dynamic tensile loading. This is important as the applications where SLM can be particularly useful, *i.e.* low run volume, high value parts as required by the aerospace, transportation and defense industries, can be expected to experience dynamic loads such as blast and high velocity impact.

One phenomenon associated with these types of event is spall fracture, or dynamic tensile damage.[11,12] Consider a situation where a plate of a material is impacted at high velocity onto another plate of the same material, known as a symmetric plate-impact. At the moment of impact, shock waves are generated and travel away from the impact interface into the flyer and sample. These shock waves are shown with red lines in figure 1a, a Lagrangian position-time plot used to track the position of waves inside the flyer plate and sample. When the shock waves reach the unsupported free surfaces of the flyer and sample they reflect back towards the impact interface as rarefaction fans, shown in black. The time of this reflection in the sample is labelled t_1, where the sample free surface accelerates to the peak velocity in figure 1b. As the flyer plate is half the thickness of the sample, the rarefaction fans intersect approximately halfway through the sample thickness. The rarefactions accelerate material in the opposite direction to their propagation, hence where they meet a region of intense tension is generated. If this tension is sufficient it will nucleate voids in the sample, which grow and coalesce to form a spall plane, highlighted blue. In the free surface velocity plot, the onset of the rarefaction fan reaching the sample surface results in a deceleration (t_2), which if no spall occurred would mean the free surface velocity would reduce to almost zero. However, if spall does occur, another compressive wave propagates from the spall plane and reaches the surface at t_3. This difference in free surface velocity be-

[a)] djones@lanl.gov

tween t_2 and t_3 is known as the pullback velocity, and is used to calculate the spall strength (resistance to spall fracture) as discussed in detail in section IV A.

The response of wrought Ti-6Al-4V to this type of plate-impact driven spall fracture has been extensively studied.[13–18] The purpose of the work presented here was to investigate both how additively-manufactured Ti-6Al-4V performs compared to wrought and whether the AM process provokes an anisotropic spall strength.

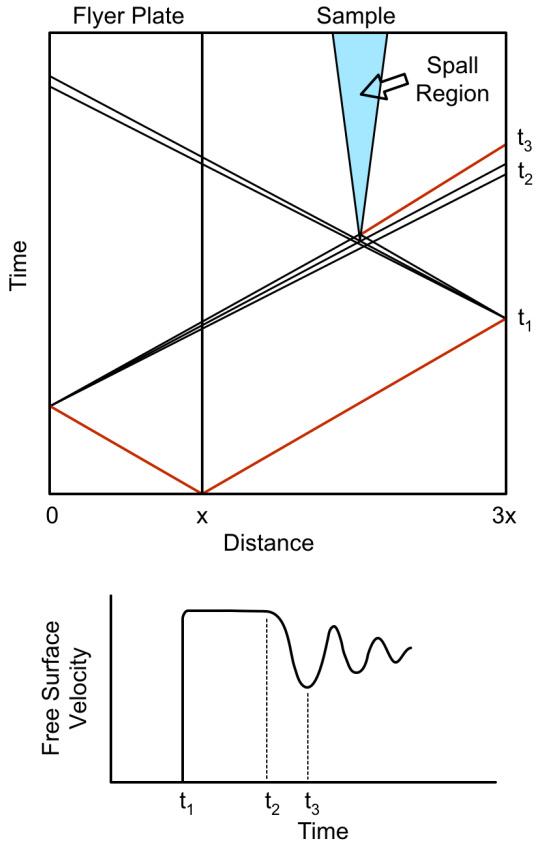

FIG. 1. Idealized case of the symmetric plate-impact experiment, neglecting elastic waves. a) Lagrangian x-t plot (position-time) tracking the shock (red) and rarefaction (black) waves, showing how they lead to a region of spall fracture (blue). b) A representative free-surface velocity plot (measuring at position 3x in the x-t plot) showing how the internal events present at the sample surface as a spall signal.

II. MATERIAL

Two pieces of SLM Ti-6Al-4V were supplied by Proto Labs, Inc[19] produced from extra-low-interstitial (ELI) Ti-6Al-4V powder using a Concept Laser M2 powder bed AM machine. For both pieces, the laser power was 100 W and had a scan speed of 600 mm s^{-1}. A bi-directional meander scan was used, *i.e.* the laser rastered in straight rows in alternate directions, with the laser power remaining on during the turn at the end of each row. The direction of these rows was rotated by 90° after each layer was complete. This laser path is shown in figure 2a. The spacing between these rows was 105 µm, with a build layer height of 30 µm (*i.e.* 30 µm of powder was added between each build slice). The build chamber was evacuated then backfilled with argon to minimize oxygen uptake; composition analysis of the samples revealed a 0.137 percent weight oxygen content which lies within the specifications for Ti-6Al-4V (UNS R56400). Both pieces were built as rectangular cuboids with the build direction either aligned with the long edge (V-Build) or through-thickness (H-Build). A schematic of the two pieces, build layers and directions is shown in figure 2b. Further details of the build process and in-depth quasi-static testing of the final material are given by Mulay *et al.*[20]

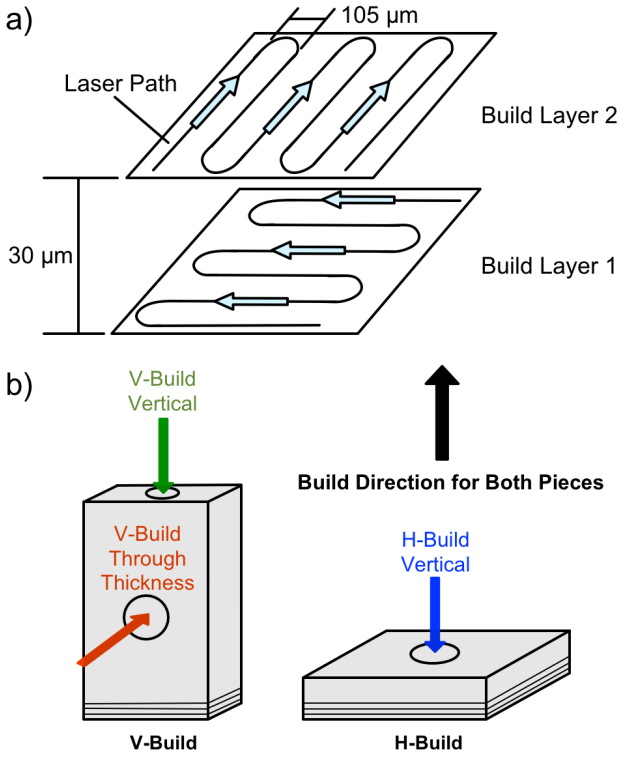

FIG. 2. The AM Ti-6Al-4V. a) The path taken by the laser, alternating between 1 and 2 as each layer is completed. b) The two pieces' build directions and sample orientations (black circles represent the disc-shaped samples, colored arrows indicate loading direction).

Electron backscatter diffraction (EBSD) was used, in addition to optical metallography, to characterize the microstructure of the as-produced plates. This revealed a microstructure composed of fine acicular or needle-like grains of α' martensite contained within much larger columnar α grains, of which the latter tended to lie parallel to the build layer interfaces. An inverse pole figure map showing these features is shown in figure 3. The metastable α' phase accounted for approximately 85 per-

cent, with α phase forming the remainder. The larger columnar grains are believed to be prior β phase grains formed during the manufacturing process, which are then rapidly cooled to produce the mixture of α and martensitic α' structure. This formation is often seen in studies of SLM Ti-6Al-4V.[3,21,22] This structure was found to be isotropic, *i.e.* imaging each direction of the fabricated parts exhibited the same acicular shaped grains.

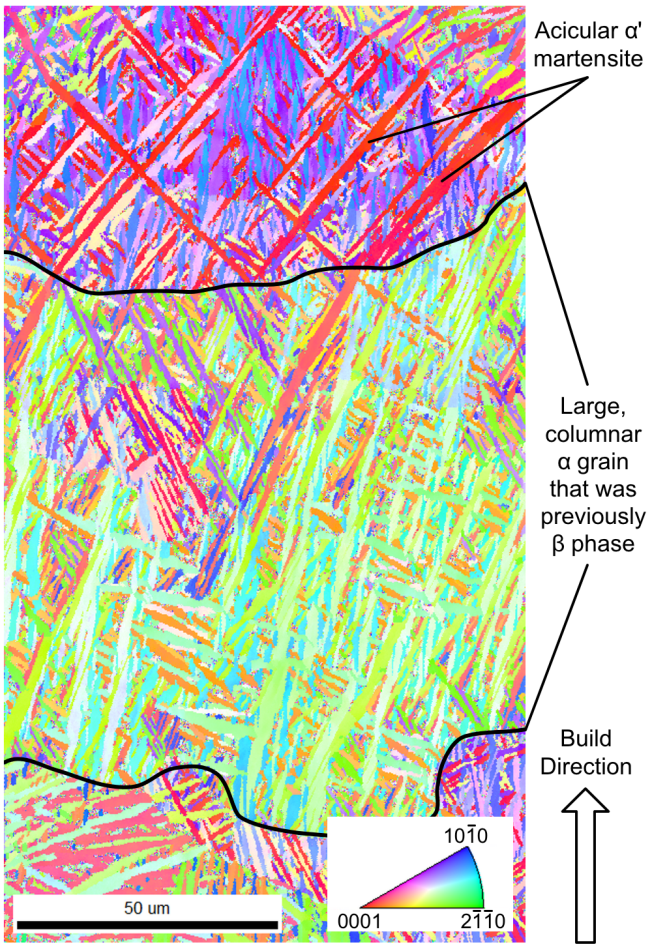

FIG. 3. Inverse pole-figure map of the AM Ti-6Al-4V, imaging along the V-build through thickness direction.

Quasi-static (strain rate of $10^{-3}\,\mathrm{s}^{-1}$) compressive and tensile tests were performed at room-temperature on the AM Ti-6Al-4V. The tests were carried out with the force applied either along the build direction (V-Build vertical, V-V) or normal to the build direction (V-Build through-thickness, V-TT). Hence the applied stress was either across (V-V) or along (V-TT) the build layer interfaces. The results of these tests are plotted in figure 4.

These data show that samples where the prior β boundaries are parallel to the tensile axis (V-TT) exhibited greater ductility as evidenced by the increased reduction in area and slightly higher elongation to failure as shown in Table I. This behavior has been observed

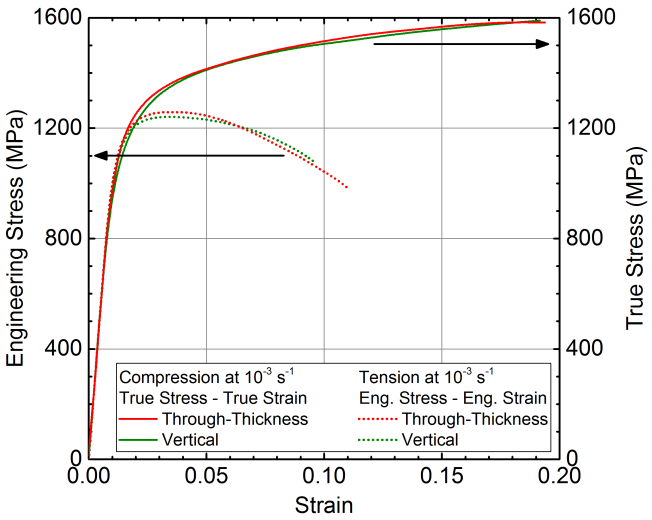

FIG. 4. Quasi-static test data for the AM Ti-6Al-4V. Solid lines / right y-axis: true stress - true strain compression. Dotted lines / left y-axis: engineering stress - engineering strain tension. Colors match loading directions in figure 2a.

in similar tests on additive manufactured Ti6Al4V.[23] The elastic modulus and yield stress of the two orientations, however, are virtually identical.

TABLE I. Quasi-static tensile test results.

Tensile Loading Direction	Elastic Modulus (GPa)	Yield Strength (MPa)	Elongation to Failure (%)	Area Reduction (%)
V-TT	110.0 ± 0.7	1072 ± 11	10.9 ± 0.7	35.9 ± 3.9
V-V	111.0 ± 0.4	1089 ± 25	8.8 ± 1.5	23.2 ± 6.3

III. EXPERIMENT

A series of symmetric plate-impact experiments were performed on an 80 mm bore single stage gas-gun. The flyer plates were machined from wrought Ti-6Al-4V, 2 mm thick, and mounted to the front of a sabot. A low density glass-microbead foam was inserted behind the flyer, to provide support and avoid bowing during the projectile acceleration. This allows an almost full stress-release in the flyer plate. Disc-shaped targets were machined from the AM Ti-6Al-4V pieces, as shown by the colored arrows and black circles in figure 2b. These were 4 mm thick (twice that of the flyer plate) to place the spall plane in the center of the target thickness, as demonstrated in figure 1. The spall plane is parallel to the impact plane, *i.e.* the tensile force acts along the impact direction. Hence the AM samples will have two orientations between their build layer interfaces and the applied tension, in the V-build vertical and H-build ver-

tical cases the tension will be normal to the layer interfaces. In the V-build through thickness sample the tension will be applied along or parallel to the layer interfaces. These directions were chosen to compliment the quasi-static data, where applying tension across the layer interfaces resulted in reduced ductility, to see if the same patterns were followed at dynamic strain-rates. Targets were also machined from wrought Ti-6Al-4V to act as a control. All targets were mounted in 'momentum rings', to avoid edge release waves from further damaging the sample after impact and ensure that any internal damage seen when the targets were sectioned post-mortem was primarily caused by a single tensile loading. This technique has been described in detail by Gray.[24] Two projectile velocities were used, $310\,\mathrm{m\,s^{-1}}$ and $415\,\mathrm{m\,s^{-1}}$. These produced peak longitudinal stresses in the targets of 3.7 GPa and 4.9 GPa respectively, chosen from reviewing the literature to produce two different levels of incipient damage. This would avoid the rear spall plate completely separating from the target, which would have hindered soft-recovery and post-mortem analysis. The lower velocity experiment had all four samples within one target assembly. For the higher velocity experiment two shots with two samples each were fired, hence the small difference in peak free surface velocity due to a slightly different ($\sim 10\,\mathrm{m\,s^{-1}}$) flyer velocity. The rear free surface velocity of each sample and the projectile velocity was measured using photon Doppler velocimetry (PDV).[25] A schematic of the experimental setup and the location of the PDV probes is shown in figure 5.

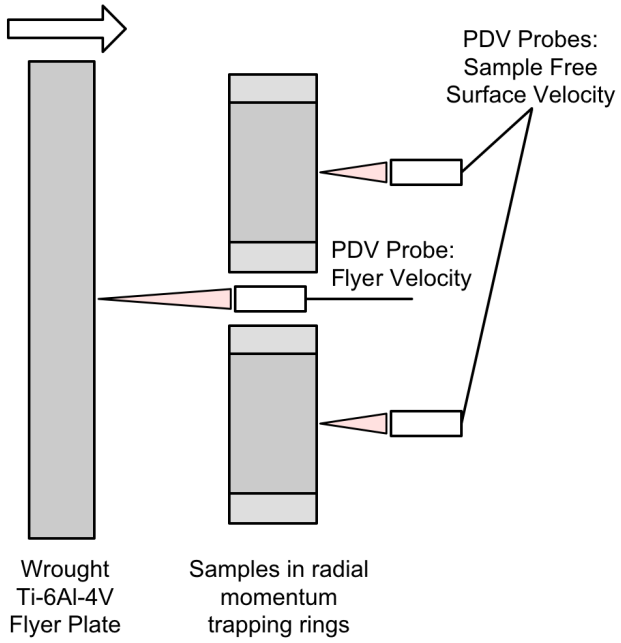

FIG. 5. Schematic of the experimental setup (not to scale). Flyer plate moves from left to right and impacts the four samples (two shown), with PDV measuring the flyer plate velocity and the samples' free surface velocitiy.

IV. RESULTS AND DISCUSSION

The free surface velocity histories were reduced from the PDV signals with the contemporary short-time Fourier transform method.[26] These are plotted in figure 6 for the $310\,\mathrm{m\,s^{-1}}$ flyer velocity data on the left and $415\,\mathrm{m\,s^{-1}}$ on the right. The line colors match the arrows indicating loading direction in figure 2. Each velocity trace has an initial elastic wave followed by approximately 0.5 µs at the peak stress state. Noise in the early time data made resolving the elastic wave velocity difficult in all but the bar stock samples, with the measured Hugoniot elastic limit of 2.7 GPa consistent with the values in the literature.[27]

A. Free Surface Velocity Measurements

The spall strength, σ_{sp}, is related to the magnitude of the pullback in the free surface velocity after the peak shock state. The original form of Novikov[28] was used with a correction due to the fact that we observed internal damage at a free surface and the signals will be distorted by having to propagate through material to reach this surface:[29]

$$\sigma_{\mathrm{sp}} = \frac{1}{2}\rho_0 c_B \left(\Delta u_{\mathrm{fs}} + \delta\right), \tag{1}$$

$$\delta = \left(\frac{h_{\mathrm{sp}}}{c_B} - \frac{h_{\mathrm{sp}}}{c_L}\right) \cdot \frac{|\dot{u}_1| \cdot |\dot{u}_2|}{|\dot{u}_1| + |\dot{u}_2|}, \tag{2}$$

where ρ_0 is the initial density, c_B is the bulk sound speed, Δu_{fs} is the pullback in free surface velocity, h_{sp} is the distance from the spall plane to the rear free surface and $\dot{u}_1$ and $\dot{u}_2$ are the gradients of the deceleration and acceleration phase of the spall pullback signal respectively. The calculated values of σ_{sp} for each shock direction are given in table II.

TABLE II. The spall strength and void percentage of each loading direction for the two flyer velocities.

Flyer Velocity ($\mathrm{m\,s^{-1}}$)	Loading Direction	Spall Strength σ_{sp} (GPa)	Damage Fraction of Spall Region
310 ± 10	Wrought	n/a	0
	V-TT	n/a	0.3 ± 0.3
	H-V	3.03 ± 0.06	1.7 ± 0.3
	V-V	2.92 ± 0.06	1.0 ± 0.3
415 ± 10	Wrought	5.28 ± 0.11	2.5 ± 0.3
	V-TT	5.03 ± 0.10	4.0 ± 0.3
	H-V	3.34 ± 0.07	8.6 ± 0.3
	V-V	3.04 ± 0.06	9.1 ± 0.3

It is clearly apparent that there is a large difference in spall strength between the AM samples that

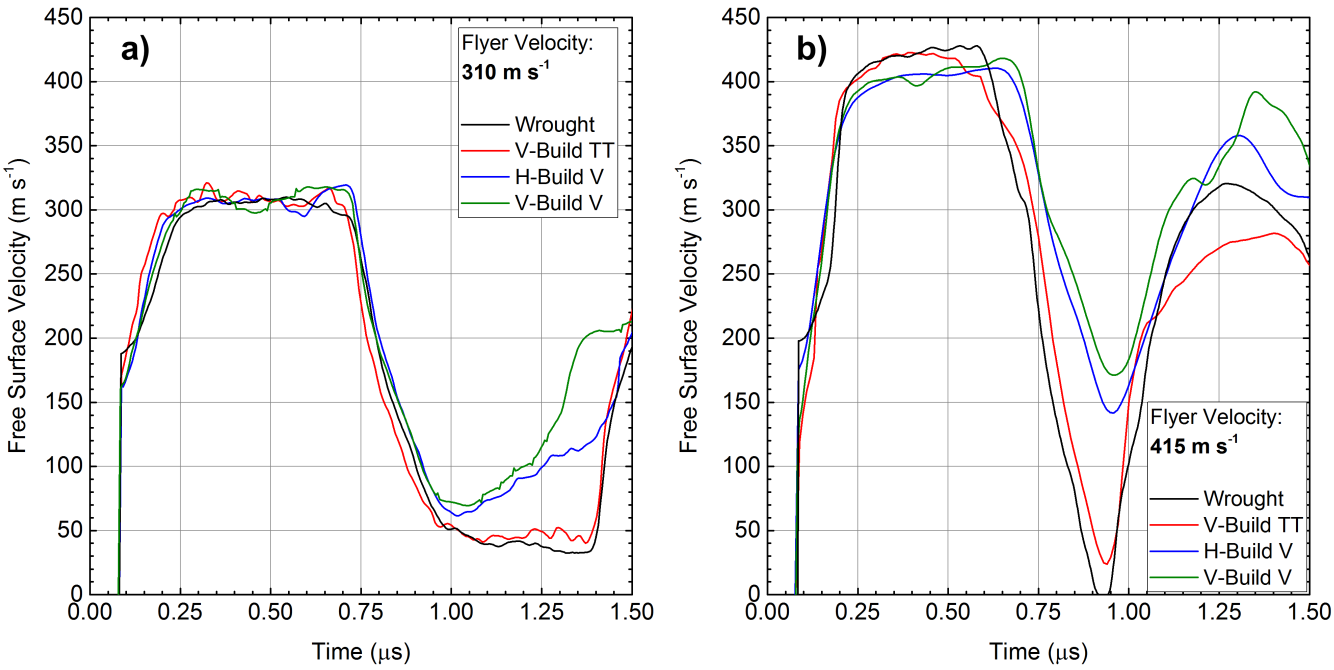

FIG. 6. Sample free surface velocity histories for the two flyer velocities; a) 310 m s^{-1} and b) 415 m s^{-1}. Colors for the additive samples match the direction arrows in figure 2.

were loaded in the through-thickness and vertical directions, with the latter exhibiting a much lower resistance to spall. At the lower flyer velocity of 310 m s^{-1}, the wrought control and the through-thickness samples showed no pullback signal indicative of spall, whereas the H-Build and V-Build vertically loaded AM samples had spall strengths of 3.03 ± 0.06 GPa and 2.92 ± 0.06 GPa, respectively. When the flyer velocity was increased to 415 m s^{-1} all four samples had a pullback signal in the free surface velocity data. The wrought control had a spall strength of 5.28 ± 0.11 GPa with the through-thickness AM sample again exhibiting a response very similar to the wrought at 5.03 ± 0.10 GPa, or 95 percent of the wrought. In contrast, the H-Build and V-Build vertical AM samples had values of just 3.34 ± 0.07 GPa and 3.04 ± 0.06 GPa, around 60 percent of the wrought control. The portion of the velocity data where the free surface velocity increases after the minima reached during pullback was extracted for the samples that spalled, then shifted to start at zero velocity and time. This data is plotted in figure 7. Dotted lines and labels representing the approximate slope of these reload signals have also been added.

The gradient of this velocity increase can be used to infer the damage kinetics of the spall process.[12] For the 415 m s^{-1} shots, the responses can be grouped into similar pairs - the wrought and through-thickness samples compared to the two vertical samples. The initial slope of the reloading signal represents the void growth phase where the nucleated voids increase in size. At a later time the slope decreases as these voids coalesce, a slower mechanism than the growth phase. Initially the wrought and AM through-thickness have the same reload rate but the through-thickness sample transitions to the coalescence phase earlier. The other two samples, the vertical

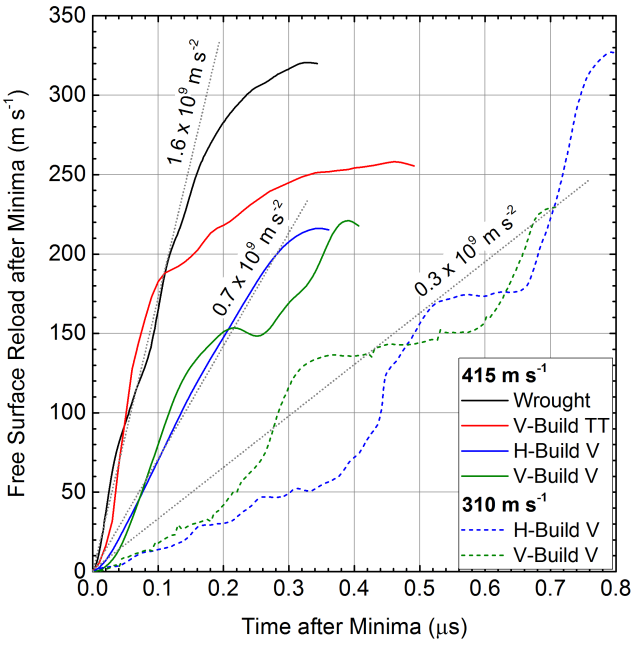

FIG. 7. The reloading sections of the spall signals. Grey dotted lines and labels represent the approximate gradients of the reloads.

directions, have a much shallower reload from the onset. Our hypothesis is that this is due to the different orientation between the tensile stress direction and the AM build layer interfaces. It has been shown that microstructural features such as grain boundaries can reduce the spall strength of a material, acting as nucleation sites for voids.[30–32] The EBSD analysis in section II showed that the SLM process in Ti-6A;-4V can produce a preferential alignment between long, columnar grain boundaries and the build layers. In the vertically loaded AM samples, tension was applied across these weaker interfaces, allowing a large number of voids and cracks to nucleate in a very short time period (see figure 8b). Hence the majority of the reload signal represents these voids linking along the layer interfaces in a delamination and cracking process. This creation of a large number of voids and void linkage rapidly reduced the tensile stress available to drive void growth, resulting in the shallower reload signal of the vertically loaded samples.
[30–32]

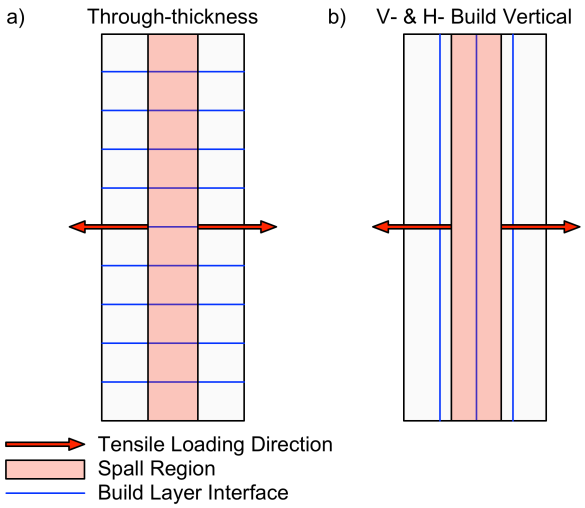

FIG. 8. The orientations between the tensile loading direction (arrows) and the build layers (blue lines) for the SLM samples.

In contrast, most of the tensile stress in the through-thickness direction AM sample was applied to material between interfaces (figure 8a) so we were effectively probing the response of the bulk AM microstructure, resulting in an initial reload signal very similar to that of the wrought material. As the voids grew, the stress state moved away from simple 1D tension and allowed shear stresses to act across the weaker build layer interfaces, hence the through-thickness sample entered the coalescence phase earlier than the wrought and the reload slope decreased. As spall strength is calculated from the magnitude of the velocity pullback, which is dominated by the void nucleation, the through-thickness AM sample exhibits a spall strength some 95 percent of wrought, even though the amount of internal damage is quite different (discussed further in section IV B).

At the lower flyer velocity, the vertically-loaded AM samples showed a stepped reloading. The reduced impact velocity meant both the tensile stress and strain-rate were lower. Hence the overall slope of the reload signals was reduced as there was less tension to drive void growth. The slower rate also meant that void nucleation was less localized and multiple fracture planes could form, with each step in the reload representing void growth and coalescence occurring at different depths in the sample being communicated to the rear free surface.

B. Damage Analysis

The recovered spallation samples were sectioned across the diameter to allow the internal damage evolution to be characterized with optical microscopy. The images of the spall planes are shown in figure 9 for both flyer velocities. To quantify the amount of damage a region at the center of each image 5 mm wide by 2 mm high was chosen, represented by the dashed boxes in figure 9. These sections were analyzed with the ImageJ software package. They were first converted to greyscale, then a threshold applied to only select dark regions corresponding to voids and regions of coalescence while ignoring other features such as grain boundaries. The image was then converted to binary such that a particle size analysis could be run and the area of each void measured. The sum of the damage area in the dashed box for each sample is listed in the final column of table II.

At $310\,\mathrm{m\,s^{-1}}$ only the vertically-loaded AM samples showed a pullback signal, although the microscopy revealed a very small amount of damage in the through-thickness AM sample along the expected spall region. Both the H-Build and V-Build vertical AM samples showed a series of fine horizontal fractures and voids spread over a large fraction of the sample thickness. As each one of these failure sites activated, it would propagate as a loading / deceleration to the sample surface rear producing the stepped velocity history. The spall strength and void / fracture area percentage was approximately the same for both vertical AM samples.

When the flyer velocity was increased to $415\,\mathrm{m\,s^{-1}}$ all the spallation samples had a spall signal in the velocity data. The spall plane in the wrought sample is typical of that seen in the literature, with the majority of damage placed in horizontal bands (normal to the tensile loading direction) linked by smaller shear fractures.[13] The area analyzed optically showed a damage fraction of 2.5 ± 0.3 percent. The through-thickness AM sample has a very similar pattern but an increased amount of damage (4.0 ± 0.3 percent). The sub-fractures linking the horizontal planes appear to be more steeply angled, *i.e.* tending to lie along the build layer interfaces as suggested in the hypothesis regarding the reloading signals. As discussed earlier, the vertical AM samples had a much reduced spall strength compared to the wrought and through-thickness AM sample by some 40 percent. The optical images showed the damage in the vertical AM

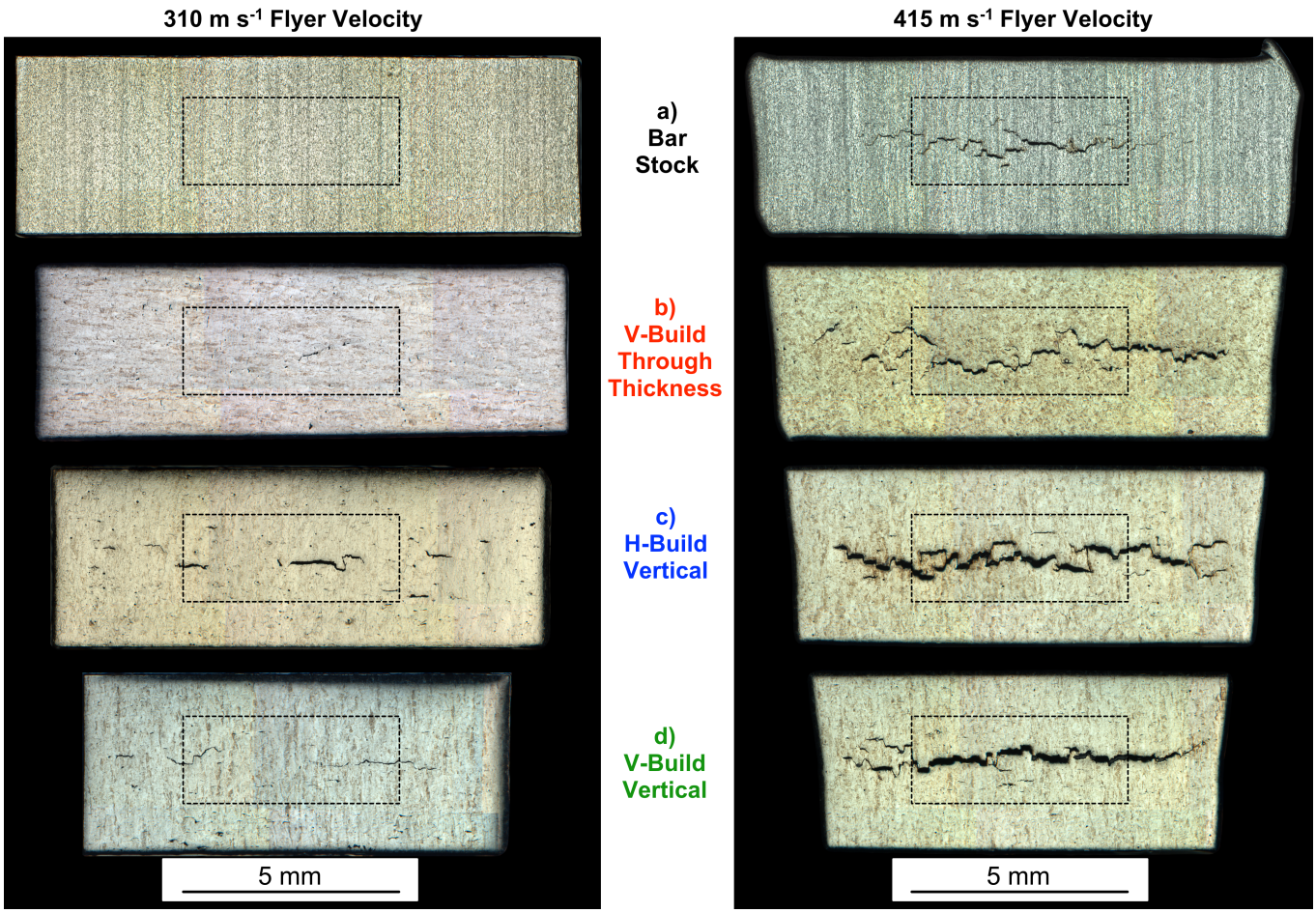

FIG. 9. Optical micrographs of the recovered samples. The dashed boxes mark the 5 mm by 2 mm region used in the damage analysis.

samples to be more confined, that is while the damage amount was higher at around 9 percent it was more localized around a spall plane in the center of the AM sample thickness. The fractures had also opened much wider than in the wrought and AM though-thickness samples. Again, this is consistent with the hypothesis that the void nucleation occurs very quickly on the weaker AM build layer interfaces, followed by a period of delamination along these boundaries. Further evidence of this is the fractures being longer horizontally than the wrought and AM through-thickness samples, indicating the nucleation occurs over a very short timescale when the rarefaction waves first interact in a narrow region at the center and the coalescence takes place along the layer boundaries.

V. CONCLUSIONS

A series of gas-gun launched flyer-plate-impact spallation experiments were fielded to investigate the directional dependence of the spall strength in additively manufactured Ti-6Al-4V. Two pieces of material were produced through selective laser melting such that the tensile stress created by the plate impact experiment could be aligned along or normal to the interfaces between build layers. A sample of wrought Ti-6Al-4V was used as a control. Two flyer velocities were used, $310\,\mathrm{m\,s^{-1}}$ and $415\,\mathrm{m\,s^{-1}}$, to generate different magnitudes of tensile stress. PDV was used to measure the samples' rear free surface velocity to allow spall strength to be calculated, alongside soft recovery such that the internal damage evolution could be characterized.

The results showed a large reduction in spall strength and an accompanying increase in damage when the tensile stress was acting normal to the AM build layer interfaces, that is the H-Build and V-Build vertical AM samples. At the lower impact velocity, the wrought and AM through-thickness samples did not exhibit a characteristic spall signal in the free surface velocity data, where the vertical AM samples had spall strengths around 3 GPa. Increasing the impact velocity initiated spall in all of the AM and wrought samples, with spall strengths of 5 GPa in the through-thickness AM sample and again approxi-

mately 3 GPa in the vertical AM samples. Analysis of the reloading signals and the optical microscopy suggested that when the tensile stress acts normal to the AM build layer interfaces void nucleation and fracture occurs very quickly on these weaker planes, followed by a delamination cracking and fracture process along the interfaces. The result is a damage region that is more concentrated but contains much wider fractures. When the tensile stress is applied in the same direction as the AM layer interfaces such as in the through-thickness AM sample, the initial response is very similar to the wrought sample as we are effectively acting on the bulk microstructure and not on the weaker interfaces. At late times where the stress state is no longer one dimensional, the AM build layer interfaces influence the spall by facilitating easier linking between existing spall planes.

The weaknesses resulting from the SLM manufacturing process were much more pronounced in the dynamic tests compared to the quasi-static tests. While the tensile tests found the vertical loading direction to fail at some 20 percent less elongation than the through-thickness loading, the difference in spall strength between these directions was up to 40 percent at the higher impact velocity. This highlights the importance of rate-dependent studies when characterizing new materials and manufacturing techniques. Future work will investigate how changes in the material production, both during manufacture such as laser power, raster speed etc. and post manufacture such as heat treating can help reduce the directional dependence and bring the SLM Ti-6Al-4V closer to a wrought Ti-6Al-4V response. Work at lower impact velocities (and hence eventual tensile stresses) to produce samples with very early time damage will help to identify where voids are nucleating, helping to reinforce our hypothesis that the build layer interfaces act to promote void formation.

ACKNOWLEDGMENTS

Los Alamos National Laboratory is operated by Los Alamos National Security, LLC, for the National Nuclear Security Administration of the U.S. Department of Energy under Contract No. DE-AC52-06NA25396. This work was partially sponsored by the Joint DoD/DoE Munitions Technology Development Program. Part of this work was performed under the auspices of the U.S. Department of Energy by Lawrence Livermore National Laboratory under Contract DE-AC52-07NA27344.

[1]K V Wong and A Hernandez. A Review of Additive Manufacturing. *ISRN Mechanical Engineering*, 2012(4):1–10, 2012.

[2]J-P Kruth, G Levy, F Klocke, and T H C Childs. Consolidation phenomena in laser and powder-bed based layered manufacturing. *CIRP Annals - Manufacturing Technology*, 56(2):730–759, January 2007.

[3]L E Murr, S A Quinones, S M Gaytan, M I Lopez, A Rodela, E Y Martinez, D H Hernandez, E Martinez, F Medina, and R B Wicker. Microstructure and mechanical behavior of Ti–6Al–4V produced by rapid-layer manufacturing, for biomedical applications. *Journal of the Mechnical Behavior of Biomedical Materials*, 2:20–32, 2009.

[4]T Vilaro, C Colin, and J D Bartout. As-Fabricated and Heat-Treated Microstructures of the Ti-6Al-4V Alloy Processed by Selective Laser Melting. *Metallurgical and Materials Transactions A*, 42(10):3190–3199, May 2011.

[5]L E Murr, S M Gaytan, D A Ramirez, E Martinez, J Hernandez, K N Amato, P W Shindo, F R Medina, and R B Wicker. Metal fabriaction by additive manufacturing using laser and electron beam melting technologies. *Journal of Materials Science & Technology*, 28(1):1–14, January 2012.

[6]H Khalid Rafi, T L Starr, and B E Stucker. A comparison of the tensile, fatigue, and fracture behavior of Ti–6Al–4V and 15-5 PH stainless steel parts made by selective laser melting. *Int J Adv Manuf Technol*, 69(5-8):1299–1309, June 2013.

[7]C Qiu, NJ E Adkins, and M M Attallah. Microstructure and tensile properties of selectively laser-melted and of HIPed laser-melted Ti-6Al-4V. *Mater. Sci. Eng. A-Struct.*, 578:230–239, 2013.

[8]P Edwards and M Ramulu. Fatigue performance evaluation of selective laser melted Ti-6Al-4V. *Mater. Sci. Eng. A-Struct.*, 598:327–337, 2014.

[9]M Simonelli, Y Y Tse, and C Tuck. Effect of the build orientation on the mechanical properties and fracture modes of SLM Ti-6Al-4V. *Mater. Sci. Eng. A-Struct.*, 616:1–11, 2014.

[10]R Fadida, D Rittel, and A Shirizly. Dynamic Mechanical Behavior of Additively Manufactured Ti6Al4V With Controlled Voids. *J. Appl. Mech.*, 82(4):041004, 2015.

[11]T Antoun, L Seaman, D R Curran, G I Kanel, S V Razorenov, and AV Utkin. *Spall Fracture*. Springer Verlag, 2003.

[12]G I Kanel. Spall fracture: methodological aspects, mechanisms and governing factors. *Int. J. Fract.*, (163):173–191, 2010.

[13]Y Me-Bar, M Boas, and Z Rosenberg. Spall studies on Ti-6Al-4V. *Mater. Sci. Eng.*, 85:77–84, 1987.

[14]G T Gray, III and C E Morris. *Influence of Peak Pressure on the Substructure Evolution and Shock Wave Profiles of Ti-6Al-4V*. LA-UR-88-625. Los Alamos National Laboratory, Los Alamos, NM, 1988.

[15]D P Dandekar and S V Spletzer. Shock Response of Ti-6AL-4V. In *AIP Conf. Proc.*, pages 427–430. AIP, March 2000.

[16]P D Church, N K Bourne, T D Andrews, and J C F Millett. Spallation in the Alloy Ti-6Al-4V. In *Shock Compression of Condensed Matter*, 2001.

[17]J C F Millett, G Whiteman, N K Bourne, and G T Gray, III. The role of anisotropy in the response of the titanium alloy Ti–6Al–4V to shock loading. *J. Appl. Phys.*, 104(7):073531, 2008.

[18]P J Hazell, G J Appleby-Thomas, E Wielewski, and J P Escobedo. The shock and spall response of three industrially important hexagonal close-packed metals: magnesium, titanium and zirconium. *Philosophical Transactions of the Royal Society A: Mathematical, Physical and Engineering Sciences*, 372(2023): 20130204–20130204, July 2014.

[19]Proto Labs Inc. Additive manufacturing: Direct laser metal sintering. `https://www.protolabs.com/additive-manufacturing/direct-metal-laser-sintering`, March 2016.

[20]R P Mulay, J A Moore, J N Florando, N R Barton, and M Kumar. Microstructure and Mechanical Properties of Ti-6Al-4V: Mill-annealed versus direct metal laser melted alloys. *Mater. Sci. Eng. A-Struct.*, 666(C):43–47, 2016.

[21]L Thijs, F Verhaeghe, T Craeghs, J Van Humbeeck, and J-P Kruth. A study of the microstructural evolution during selective laser melting of Ti–6Al–4V. *Acta Mat.*, 58(9):3303–3312, May 2010.

[22]S L Lu, H P Tang, Y P Ning, N Liu, D H StJohn, and M Qian. Microstructure and Mechanical Properties of Long Ti- 6Al-4V Rods Additively Manufactured by Selective Electron Beam Melting Out of a Deep Powder Bed and the Effect of Subsequent Hot Isostatic Pressing. *Metallurgical and Materials Transactions A*, 46(9):3824–3834, 2015.

[23]J S Keist and T A Palmer. Role of geometry on properties of additively manufactured Ti-6Al-4V structures fabricated using laser based directed energy deposition. *Materials and Design*, 106:482–494, 2016.

[24]G T Gray III. Shock-wave testing of ductile materials. In H Kuhn and D Medlin, editors, *ASM-Handbook Volume 8, Mechanical Testing and Evaluation*. ASM International, Metals Park Ohio, 2000.

[25]O T Strand, D R Goosman, C Martinez, T L Whitworth, and W W Kuhlow. Compact system for high-speed velocimetry using heterodyne techniques. *Rev. Sci. Inst.*, 77(8):083108, 2006.

[26]D H Dolan. Accuracy and precision in photonic Doppler velocimetry. *Rev. Sci. Inst.*, 81(5):053905, 2010.

[27]A Hopkins and N S Brar. Hugoniot and shear strength of titanium 6-4 under shock loading. *AIP Conf. Proc.*, 505:423–426, 2000.

[28]S A Novikov. Shear Stress and Spall Strength of Materials under Shock Loads (Review). *Journal of Applied Mechanics and Technical Physics*, 22(3):385–394, 1981.

[29]S V Razorenov, A V Utkin, G I Kanel, V E Fortov, A S Yarunichev, K Baumung, and H U Karow. Response of high-purity titanium to high-pressure impulsive loading. *High Pressure Research*, 13(6):367–376, September 1995.

[30]J P Escobedo, D Dennis-Koller, E K Cerreta, B M Patterson, C A Bronkhorst, B L Hansen, D Tonks, and R A Lebensohn. Effects of grain size and boundary structure on the dynamic tensile response of copper. *J. Appl. Phys.*, 110(3):033513, 2011.

[31]S J Fensin, S M Valone, E K Cerreta, and G T Gray, III. Influence of grain boundary properties on spall strength: Grain boundary energy and excess volume. *J. Appl. Phys.*, 112(8):083529, 2012.

[32]S J Fensin, J P Escobedo-Diaz, C Brandl, E K Cerreta, G T Gray, III, T C Germann, and S M Valone. Effect of loading direction on grain boundary failure under shock loading. *Acta Mat.*, 64(C):113–122, February 2014.